International Journal of Nanomedicine

Dovepress
Taylor & Francis Group

Open Access Full Text Article

ORIGINAL RESEARCH

Early Detection of Brain Metastases from Triple-Negative Breast Cancer with a Tumor-Targeting Dual-Modal MR/NIRF Imaging Probe

Fang Nie[1], Lin Li[2], Yingying Bai[1], Jian Yang[1,3]

[1]Department of Radiology, Nurturing Center of Jiangsu Province for State Laboratory of AI Imaging & Interventional Radiology, State Key Laboratory of Digital Medical Engineering, Zhongda Hospital, Medical School, Southeast University, Nanjing, People's Republic of China; [2]Department of Radiology, Jiangsu Province Hospital of Chinese Medicine, Nanjing, People's Republic of China; [3]Department of Physiology, Nurturing Center of Jiangsu Province for State Laboratory of AI Imaging & Interventional Radiology, State Key Laboratory of Digital Medical Engineering, Zhongda Hospital, Medical School, Southeast University, Nanjing, People's Republic of China

Correspondence: Jian Yang, Email jianyang0514@126.com

Objective: Imaging early-stage brain metastases from triple-negative breast cancer (TNBC) is challenging due to the blood–brain barrier (BBB). To address this issue, we developed Den-Angio-GE11, a nanoprobe engineered to traverse the BBB and selectively target metastatic cells.

Methods: A TNBC brain metastasis model was established in mice through intracardiac injection of MDA-MB-231 brain-seeking cells (MDA-MB-231-BR). Metastatic lesions were longitudinally monitored using T2-weighted magnetic resonance imaging (MRI) and confirmed through contrast-enhanced MRI with Gadolinium-DTPA (Gd-DTPA). The Den-Angio-GE11 nanoprobe was synthesized on a polyamidoamine (PAMAM)-G5 dendrimer platform, incorporating Angiopep-2 and GE11 peptides for BBB traversal and metastatic cell targeting. Dual-modal imaging capability was achieved by conjugating Gd-DTPA for MRI and NIR783 for near-infrared fluorescence (NIRF) imaging.

Results: Den-Angio-GE11 demonstrated significantly enhanced affinity to EGFR compared to controls, as confirmed by immunofluorescence staining and flow cytometry assays. Brain metastases appeared on T2-weighted MRI three weeks post-injection of MDA-MB-231BR cells and maintained uncompromised BBB function for another one or two weeks, as demonstrated by a lack of enhancement in Gd-DTPA-enhanced MRI. Compared to control nanoparticles, Den-Angio-GE11 remarkably enhanced T1 and NIRF signals of lesions after administration. Histological analysis confirmed Den-Angio-GE11 targeting brain metastatic cells. For lesions in extreme-early stage (undetectable by T2-weighted imaging), NIRF imaging post-Den-Angio-GE11 administration successfully indicated potential lesions. Fluorescence imaging analyses further verified Den-Angio-GE11 targeted sporadically metastatic cells in the brain parenchyma.

Conclusion: Early brain metastases of TNBC can be detected by Den-Angio-GE11 through T1-weighted MRI or NIRF imaging.

Keywords: breast cancer brain metastases, early imaging, EGFR, angiopep-2

Introduction

Brain metastases (BMs) present a substantial treatment challenge in breast cancer patients, particularly in those with triple-negative breast cancer (TNBC). TNBC, characterized by the absence of estrogen receptors (ER), progesterone receptors (PR) and human epidermal growth factor (HER2) in histochemical examination, represents the most aggressive breast cancer subtype and accounts for approximately half of all breast cancer brain metastases cases.[1,2] The blood–brain barrier (BBB) complicates early imaging and effective drug delivery, leading to a poor prognosis of brain metastasis. Patients with TNBC brain metastases have a median survival of only 4.9 months post-diagnosis, significantly shorter than

Received: 8 October 2024
Accepted: 27 February 2025
Published: 20 March 2025

the 10 to 18 months observed in other subtypes.[1,3–5] Therefore, early detection of TNBC brain metastases is crucial in clinical practice.

Crossing the BBB is essential for the efficacy of targeted nanoprobes in the molecular imaging of early-stage brain metastasis. Angiopep-2, a 19-amino acid peptide, serves as a ligand for the low-density lipoprotein receptor-related protein 1 (LRP1) on the BBB. This interaction facilitates the crossing of the barrier, enabling the delivery of therapeutic agents to the brain.[6] Angiopep-2 has been explored in preclinical studies for delivering therapeutics across the BBB in the treatment of various neurological disorders, including cancer, Alzheimer's disease, and Parkinson's disease.[7] Clinical trials have demonstrated that Angiopep-2 effectively enhances the brain penetration of paclitaxel when conjugated with drugs.[8] However, data remain insufficient regarding the capacity of Angiopep-2 to facilitate the transport of imaging probes across the BBB for early detection of brain metastases.

Identifying molecular targets remains a secondary consideration in the molecular imaging of early brain metastasis due to the limited number of recognized targets. The epidermal growth factor receptor (EGFR) is a 170 kDa transmembrane glycoprotein member of the ErbB family.[9] Studies have indicated that EGFR is frequently overexpressed in TNBC, more so than in other subtypes.[10–12] Previous research has also demonstrated that EGFR plays a significant role in the proliferation and brain metastasis of TNBC.[13,14] Moreover, EGFR has been used as a molecular target in molecular imaging and therapeutic applications. For instance, antibodies against EGFR have been conjugated with gold or fluorescent nanoparticles for computed tomography (CT) or optical imaging of lung cancers exhibiting EGFR overexpression.[15,16] The GE11 peptide, characterized by the amino acid sequence YHWYGYTPQNVI, has been shown to have high affinity for the breast cancer cell line MDA-MB-231 and the lung cancer cell lines H1299, both known for their EGFR overexpression.[17–19] Importantly, the small molecular weight of GE11 enhances its ability to cross BBB, offering significant advantages over antibodies for targeting the EGFR in the imaging of early brain metastases.

Recently, nanotechnology has demonstrated several advantages in preclinical tumor imaging, such as easy assembly, controllable particle size, tunable circulation lifetime, and enhanced permeability and retention at tumor sites.[20–22] In this study, we utilized the fifth generation (G5) polyamidoamine (PAMAM) dendrimer to develop an EGFR-targeting nanoprobe for brain metastasis imaging. Nanoparticles based on G5 PAMAM are characterized by their smaller size, high drug loading capacity, and biodegradability.[23] The nanoprobe was designed to facilitate both near-infrared (NIR) and magnetic resonance imaging (MRI) by conjugating NIR783 and Gd^{3+}-DTPA to the PAMAM dendrimer, respectively. Brain metastasis was induced in mice using MDA-MB-231 brain-seeking cells through intracardiac injection, with lesion progression monitored via T2-weighted MRI. Imaging of brain metastases with the EGFR-targeted, dual-modality nanoprobe was performed before and after the lesions were detected in T2-weighted MR images.

Materials and Methods

Materials

All chemical reagents were obtained from Aladdin Reagent (Shanghai, China) unless otherwise specified. The fifth-generation polyamidoamine dendrimer (G5 dendrimer) (MW: 28826Da) and Rhodamine-NHS were purchased from Dendritech Inc. (Midland, MI, USA). The Maleimide-PEG^{2k}-NHS and PEG-NHS were purchased from JenKem Technology Co. Ltd. (Beijing, China). GE11 peptide and Angiopep-2 were purchased from MedChemExpress (Monmouth Junction, NJ, USA). Recombinant human EGFR protein (ab155639) was from Abcam (Cambridge, MA, USA).

The human breast cancer brain-seeking cell line MDA-MB-231-BR was kindly provided by Dr. Patricia S. Steeg (National Cancer Institutes of Health, Bethesda, MD, USA). U-87 MG, BT-474 and mouse brain microvascular endothelial cell bEnd.3 were obtained from the American Type Culture Collection (ATCC). GL261 cell lines were purchased from Shanghai Zhong Qiao Xin Zhou Biotechnology Co. Ltd. (Shanghai, China). Fetal bovine serum (FBS), trypsin, penicillin and streptomycin were purchased from ThermoFisher Scientific (New York, USA).

Synthesis of the Nanoprobes

The nanoprobes were synthesized as described previously.[24] First, the fifth generation (G5) dendrimer was reacted with NHS-PEG^{2k}-OPSS (in PBS, pH=7.4) (got intermediate 1), then continued to be treated with N-hydroxysuccinimidyl (NHS) esters

of rhodamine and IR783 in PBS (pH=7.4, got intermediate 2). Subsequently, intermediate 2 was reacted with DTPA-dianhydride in $NaHCO_3$ (pH=9.5, got intermediate 4). Then, intermediate 4 was linked with Angiopep-2 or/and GE11 peptide (in PBS, pH=7.4, got intermediate 5). After that, the intermediate 5 was chelated with $Gd_2(CO_3)_3$ in HEPES (pH=8.3) to get Den-Angio or Den-Angio-GE11. Den-PEG contains G5 dendrimer, PEG, rhodamine, IR783, Gd-DTPA but not Angiopep-2 and GE11 when compared to Den-Angio or Den-Angio-GE11.

Characterization of Nanoprobes

The average molar ratios among G5 dendrimer (PAMAM), DTPA, Gd^{3+}, PEG, Angiopep-2 and GE11 in nanoprobes were determined using the ^1H NMR (Mercury 400 spectrometer, Varian, Germany). The particle size and zeta potentials were measured using a dynamic light scattering detector (Zetasizer, Malvern, USA). The binding constants between the GE11 peptides or Den-Angio-GE11 and EGFR proteins were measured using Surface Plasmon Resonance (SPR). The molecular weight of nanoprobes was determined by Gel Permeation Chromatography (GPC). The nanoparticle shape was determined by transmission electron microscopy (JEOL F200, Japan).

Cell Culture

All cell lines were maintained in Dulbecco's modified Eagle medium (DMEM) supplemented with 10% fetal bovine serum and 1% penicillin–streptomycin (complete medium). Cells were maintained at 37°C in a humidified atmosphere and 5% CO_2.

Brain Metastasis and Glioma in Mice

All animals were received care in accordance with Guide for the Care and Use of Laboratory Animals (8th edition) and approved by the Institutional Animal Use and Care Committee of the Medical School of Southeast University. Brain metastasis model was induced by intracardiac injection of MDA-MB-231-BR cells in BALB/c Nude mice (Charles River). Specifically, mice 6-week-old were housed in an SPF environment for one week with a 12-hour day/night rotation before experiments. The mice were then anesthetized by 1% isoflurane in oxygen and injected into the left ventricle (Blood pulsations were visible) with 1×10^5 MDA-MB-231BR cells in 100 μL of phosphate-buffered saline (PBS). Brain metastasis progression was monitored by T2-weighted MRI every week after injection.

The orthotopic glioma model was induced by GL261 cells in C57BL/6 mice (Charles River). Mice 6-week-old were housed for one week before experiments. The mice were then anesthetized by 1% isoflurane in oxygen and stereotaxic injected 2×10^5 GL261 cells into the brains (volume is 20 μL). The lesions of glioma were detected by T2-weighted MRI.

Cell Viability Assay

The proliferation ability of cells was assayed by CCK-8 agents. Specifically, MDA-MB-231-BR and bEnd.3 cells were collected and plated in 96-well plates at a density of 5,000 cells per well. The cells were incubated at 37°C in a 5% CO_2 atmosphere for 24 hours. After removing the supernatant, nanoprobes were diluted to designated concentrations in complete cell culture medium and added to each well. The cells were then incubated for additional 48 hours. CCK-8 (Cell Counting Kit-8, KeyGEN BioTECH, CN) was then added to each well and incubated for an additional 3 hours. The optical density of each well was subsequently measured at a wavelength of 450 nm (OD450 nm) using a microplate spectrophotometer (ThermoFisher Scientific, USA). Cell viability of normal control group was set 100%, and each group was compared with the normal control.

Invasion Assay In vitro

Invasion assays of MDA-MB-231-BR cells were conducted using invasion chambers in a 24-well plate (BD, USA). MDA-MB-231-BR cells were collected upon reaching confluency and plated into the upper chamber at a density of 50,000 cells in medium without fetal bovine serum (FBS). The lower chambers were filled with complete medium containing 20% FBS. Once cells are attached to the bottom of the upper chamber, nanoprobes were diluted to designated concentrations and added to the upper chamber. The cells were then incubated at 37°C in a 5% CO_2 atmosphere for an additional 24 hours. After

removing the supernatant, cells still attached to the bottom of the upper chamber were scratched with a cotton swab, and the migrated cells on the other side of the membrane were fixed with 4% paraformaldehyde and stained with crystal violet. The membrane was then cut down, attached to a slide, and finally examined under a microscope.

Targeting of MDA-MB-231-BR Cells

The binding rate of nanoprobes to EGFR was measured by flow cytometry analysis. MDA-MB-231-BR, U87, and BT-474 cells were collected, and the cell density was adjusted to 1×10^6 cells/mL. Triplicates of no particles, Den-Angio-GE11, Den-Angio, and Den-PEG, diluted to designated concentrations, were added to the cell suspension and incubated for 1 hour at 4°C. Following incubation, the cells were washed twice with PBS, and the binding rate was assessed through rhodamine fluorescence on the cells using the FACSCalibur analysis system (Becton Dickinson, CA, USA).

Western Blot Studies

Cells growing into confluency were lysed with RIPA buffer (ThermoFisher Scientific, USA); then, protein concentrations were quantified by BCA Protein Assay Kits (ThermoFisher Scientific, USA). The protein was subjected to SDS-PAGE and then transferred to polyvinylidenefluoride membranes (Millipore, USA). Blots were blocked with 5% skim milk (BD Bioscience, USA) and then incubated with primary antibodies to EGFR and beta-actin (Cambridge, MA, USA) overnight at 4°C. Horseradish peroxidase conjugated secondary antibodies (ThermoFisher Scientific, USA) were incubated with blots for 1 hour at room temperature. Binding was detected by chemiluminescence image analyzer (Tano, CN).

Immunofluorescence Analysis

MDA-MB-231-BR cells were seeded at approximately 2×10^4 cells per well in 12-well plates and cultured overnight to reach around 80% confluency. The nanoprobes were diluted in complete cell culture medium to designated concentrations and incubated at 37°C for 30 minutes. After incubation, the cells were washed three times with PBS and fixed with 4% formaldehyde/PBS for 10–15 minutes. The cell nuclei were stained with DAPI Fluoromount-G, and the cells were imaged using a fluorescence microscope.

Near-Infrared Fluorescence (NIRF) Imaging

For in vitro imaging, MDA-MB-231-BR cells were seeded at approximately 4×10^4 cells per well in 96-well plates and cultured overnight. The cells were then incubated with 5 μM of nanoprobes for 4 hours at 37°C. Following incubation, the cells were washed twice with PBS and then fixed with 1% Biowest Agarose for imaging.

For in vivo imaging, mice were anesthetized with a continuous supply of 1% isoflurane, subsequently injected with 100 μL of targeted or control nanoprobes through tail vessels (Each mouse was given by 0.1 μmol of probes or controls). NIRF imaging was performed at various time point (0.5, 1, 2, 4, 8, 12, 24, 36 h) using the IVIS Spectrum In vivo Imaging System (Perkin Elmer, USA). The NIRF images were collected at an excitation wavelength of 745 nm and an emission wavelength of 810 nm. To investigate the distribution of nanoprobes in mice, mice were sacrificed by dislocation of cervical vertebrae after 36 h from probes administration, and organs were taken out for imaging by NIRF.

MR Imaging

MRI was performed by a 7.0-Tesla small animal MR scanner (Bruker PharmaScan, Germany). For cell phantom imaging, 2×10^6 cells were suspended in 1 mL of 1% agarose (Oxford, UK) with 5 μmol/L nanoprobes or controls and placed in 10-mm-diameter Eppendorf tubes. A Rapid Acquisition Relaxation with Enhancement sequence (RARE) was used for T1-weighted imaging, with a repetition time of 725 ms and an echo time of 9 ms. The imaging parameters included a matrix size of 256 × 256, a field of view of 2 × 2 cm, and a slice thickness of 1 mm.

For in vivo imaging, mice were anesthetized with a continuous supply of 1% isoflurane, and their respiratory rate and body temperature were monitored using a physiology monitor. A spin echo sequence (500/9 ms of repetition time/echo time, 4 averages) was used for T1-weighted imaging, while a fast spin echo sequence (3,000/45 ms of repetition time/echo time, 3 averages) was used for T2-weighted imaging. Twelve axial slices with a slice thickness of 1 mm, a matrix of 256 × 256, and a field of view of 2 × 2 cm was positioned over the brain.

Brain Section and Staining

Mice were ordinally perfused with normal saline and 4% paraformaldehyde after anesthetization with isoflurane. Brain tissues were obtained after perfusion and fixed in formaldehyde again. Then, brain tissues were dehydrated for 48 hours in 30% sucrose solution. After that, brains were embedded by OTC and quickly frozen in liquid nitrogen. Brain tissues were cut into serial slices with 10 μm in thickness. The sections were then performed with hematoxylin and eosin staining. For fluorescence investigation, sections were washed by PBS and then stained with DAPI. Finally, sections were taken images by fluorescence microscope.

Permeability of BBB in BMS

Mice were administrated 100 μL of 2% Evans' blue via tail vein (2 mg/kg). After 12 hours, mice were anesthetized with isoflurane and perfused with normal saline. Brain tissues were dissected, and 100 mg of tissue was minced and then incubated in dimethylformamide at 60°C for 24 hours. The supernatants were subsequently obtained by centrifugation at 1000 revolutions per minute, and the absorbance was measured at 620 nm.

Statistical Analysis

The statistical analysis was performed using SPSS Statistics 20 software. Numerical data are expressed as means ± standard deviations (SD). For statistical comparisons, an independent-sample *t*-test was employed. A P value less than 0.05 was considered statistically significant.

Results

Synthesis and Characterization of the Nanoprobes

The chemical structures and synthetic pathways of nanoprobes are presented in Figure 1. Briefly, the PAMAM G5 dendrimer was selected as a platform and modified with polyethylene glycol to enhance biocompatibility and prolong the half-life in circulation. The rhodamine and NIR fluorophore NIR783 were conjugated to enable visualization of brain sections in vitro and NIR imaging of the brain in vivo. Then, the EGFR targeting peptide GE11 and BBB-permeable angiopep-2 were functionalized into the PAMAM dendrimer. Additionally, Gd^{3+}-DTPA was synthesized to the dendrimer for MR imaging due to its high thermodynamic stability and kinetic inertness.

The key physical and chemical properties of the nanoprobes were listed in Table 1. It is shown that the average hydrodynamic diameter of the nanoprobe Den-Angio-GE11 was about 8.8nm, which was slightly larger than that of the control groups Den-Angio (7.3 ± 0.16 nm) and Den-PEG (5.7 ± 0.18 nm) (Figure S1). The polydispersity index (PDI) of all nanoprobes was below 0.3, and the surface charges ranged from +7.3 to +7.8 mV (Figure S1). The shape of Den-PEG, Den-Angio and Den-Angio-GE11 was close to circular as shown in Figure S2. The molecular weight of Den-Angio-GE11 was approximately 115 kDa. The molar ratios of PAMAM/DTPA/Gd/PEG/Angiopep-2/GE11 in Den-Angio-GE11 were 1/84/41/12.6/4.5/6.7 calculated according to the data of ^{1}H NMR Den-PEG, Den-Angio and Den-Angio-GE11 (Figure S3). The T1-weighted relaxation times of nanoprobes ranged from 82.9 to 90.3 ms.

Cytotoxicity of Nanoprobes

The cytotoxicity of the nanoprobes was evaluated by measuring the viability of MDA-MB-231-BR and mouse brain endothelium cells bEnd.3. As shown in Figure 2A and B, cell viability was not significantly declined, as the nanoprobe concentration gradually increased. At a nanoprobe concentration of 10 μM, the cell viability of bEnd.3 cells was approximately 94% compared to the normal control, indicating negligible cytotoxicity of the nanoprobes in vitro.

Furthermore, the effect of nanoprobes on the invasion of MDA-MB-231-BR cells was assessed. As shown in Figure 2C and D, Den-Angio-GE11 and its control nanoprobes, Den-Angio and Den-PEG, did not significantly affect metastatic cell invasion.

https://doi.org/10.2147/IJN.S498629

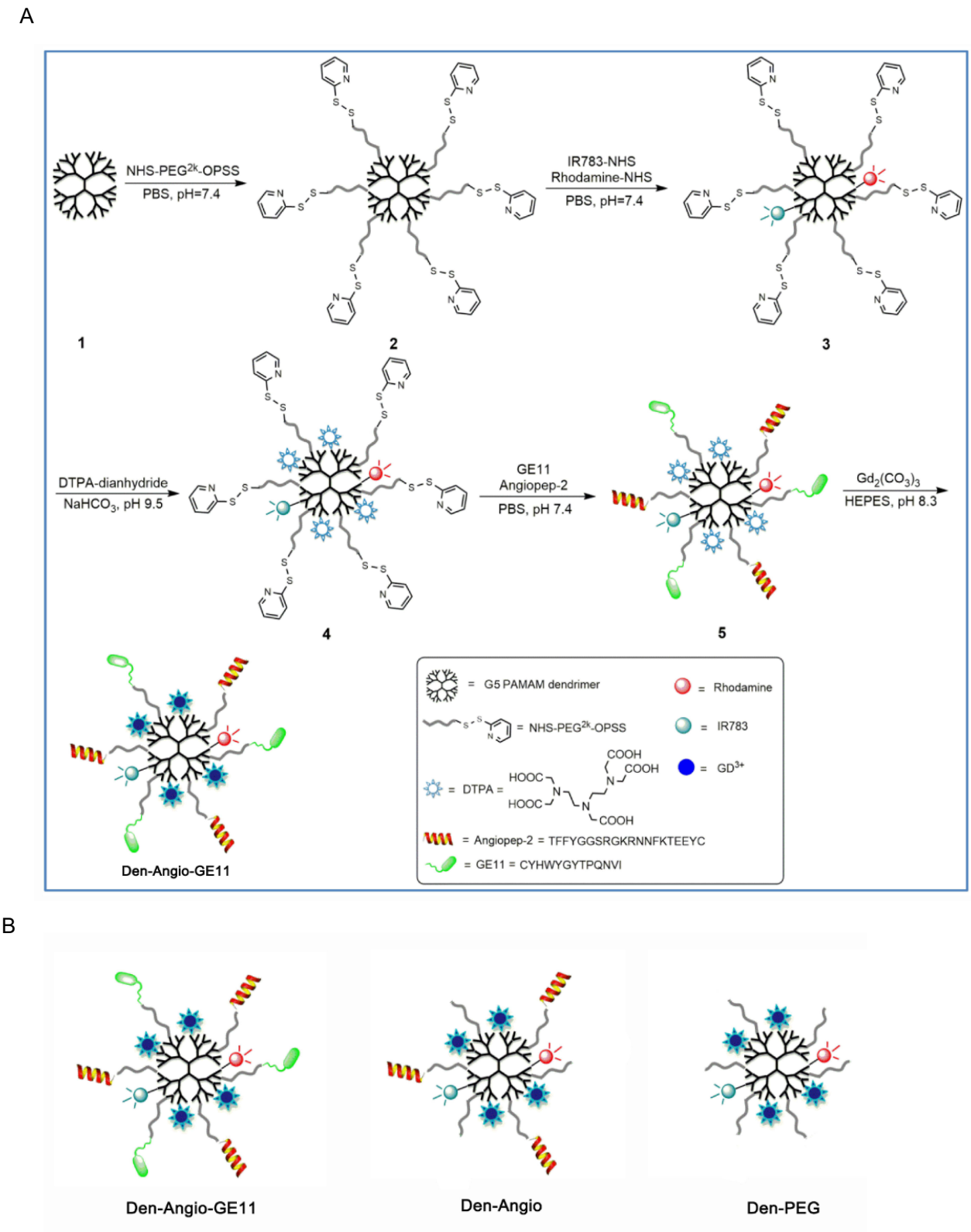

Figure 1 Construction of EGFR-targeted nanoprobe and control nanoprobes. (**A**) Schematic illustration of the nanoparticle synthesis route. (**B**) Structures of the EGFR-targeted nanoprobe Den-Angio-GE11 and control probes Den-Angio and Den-PEG.

Table 1 Physical Parameters of the Nanoprobes

Nanoprobes	*d* (nm)[a]	*PDI*[a]	*ζ*[a]*(mV)*	*Mw (kDa)*[c]	T1-Weighted Relaxivitives (msec)[d]	Molar Ratios[b]
Den-PEG	5.7	0.28	+7.8	93	85.5	1/84/41/12.6/0/0
Den-Angio	7.3	0.19	+7.7	104	90.3	1/84/41/12.6/4.5/0
Den-Angio-GE11	8.8	0.24	+7.3	115	82.9	1/84/41/12.6/4.5/6.7

Notes: [a]The hydrodynamic diameter (d), polydispersity index (PDI), and zeta potentials (ζ) were measured by dynamic light scattering (DLS). [b]Molar ratios between G5 dendrimer, DTPA, Gd, PEG, Angiopep-2 and GE11 in nanoprobes were measured by the characteristic protons in ^{1}H NMR. [c]Molecular weights (MW) were measured by MALDI-TOF MS. [d]T1-weighted relaxivities (r1p) were determined on 7.0 T MRI at 25°C.

Targeting of Nanoprobes to EGFR

The physical affinity of nanoprobes for MDA-MB-231-BR cells was tested in vitro using Surface Plasmon Resonance (SPR). The dissociation constant of the nanoprobe Den-Angio-GE11 was 8.344×10^{-10} mol/L (M), significantly lower than GE11 peptide (7.946×10^{-7} M) (Figure 3A). Immunofluorescence staining results indicated a dose-dependent increase in red fluorescence signals in the Den-Angio-GE11 group, while no significant increase was observed in the control group (Den-Angio and Den-PEG) (Figure 3B). Flow cytometry quantification showed that the binding of Den-Angio-GE11 to MDA-MB-231-BR cells reached 64.2% at 5 μmol/L, which was significantly higher than that of the control groups (Figure 3C and D, $P<0.05$).

Further, to verify the specificity of this binding, the binding ratio of Den-Angio-GE11 was also assayed in EGFR-low expressed BT-474 cells and moderately expressing U87 cells (Figure 3E). As shown in Figure 3F, the binding ratio of Den-Angio-GE11 at 5 μM was 0.7% with BT-474 and 47.5% with U87 cells, respectively. The statistics result indicated that the binding rate of Den-Angio-GE11 with MDA-MB-231-BR cells was significantly higher than that with BT-474 cells (Figure 3G), which supported the specific recognition of MDA-MB-231-BR cells by Den-Angio-GE11.

Imaging Capability in Vitro of Nanoprobes

The imaging capability of nanoprobes was first investigated in MDA-MB-231 BR cells. When incubated with Den-Angio-GE11 and control vectors for 5 minutes (the time at which the binding ratio reached its maximum), MDA-MB-231 BR cells exhibited significantly higher signal intensity on T1-weighted MRI compared to the control nanoprobe groups or the PBS group (Figure 4A and B, $P<0.05$). Similarly, NIR imaging results (Figure 4C and D, $P<0.01$) indicated that the Den-Angio-GE11 group had significantly higher fluorescence intensity than the control nanoprobe groups and the PBS control group. These assays demonstrated that Den-Angio-GE11 could image metastatic MDA-MB-231-BR cells.

BBB Permeability in Mice With Brain Metastasis

The brain metastases in mice were monitored by T2-weighted MRI on days 7, 14, 21, 24, 28 and 35 after brain metastases induced. When lesions were detected in T2-weighted images, BBB permeability was evaluated using Gd-DTPA-enhanced T1-weighted MRI. As Figure 5A shown, six lesions were detected in all mice by T2-weighted images on day 21 after brain metastases preparation. On day 24, seventeen lesions (about one-half of total lesions) appeared on T2-weighted images. And on day 35, total 30 lesions appeared on T2-weighted images in our study (10 mice in BMS group). The BBB permeability was evaluated weekly through T1-enhancement by Gd-DTPA. In addition to two lesions that were enhanced by Gd-DTPA on day 21, most lesions will be enhanced after day 35. Some individual lesions remained non-enhancement even on day 50 (Figure 5B and C). This result indicates that brain metastasis induced by MDA-MB-231-BR cells progressed slowly in the early stage and BBB in this model remained functions for one or two weeks after detection by T2-weighted MRI. In contrast, glioma lesions were enhanced by Gd-DTPA on day 7 after grafting. Results of Evans' blue leakage assay showed that, in most cases of brain metastases, BBB was functional before day 35 (Figure 5E) in this study. Histological examination revealed that the metastatic cells clustered in the hyperintense area on T2-weighted images, separated by numerous voids (Figure 5D).

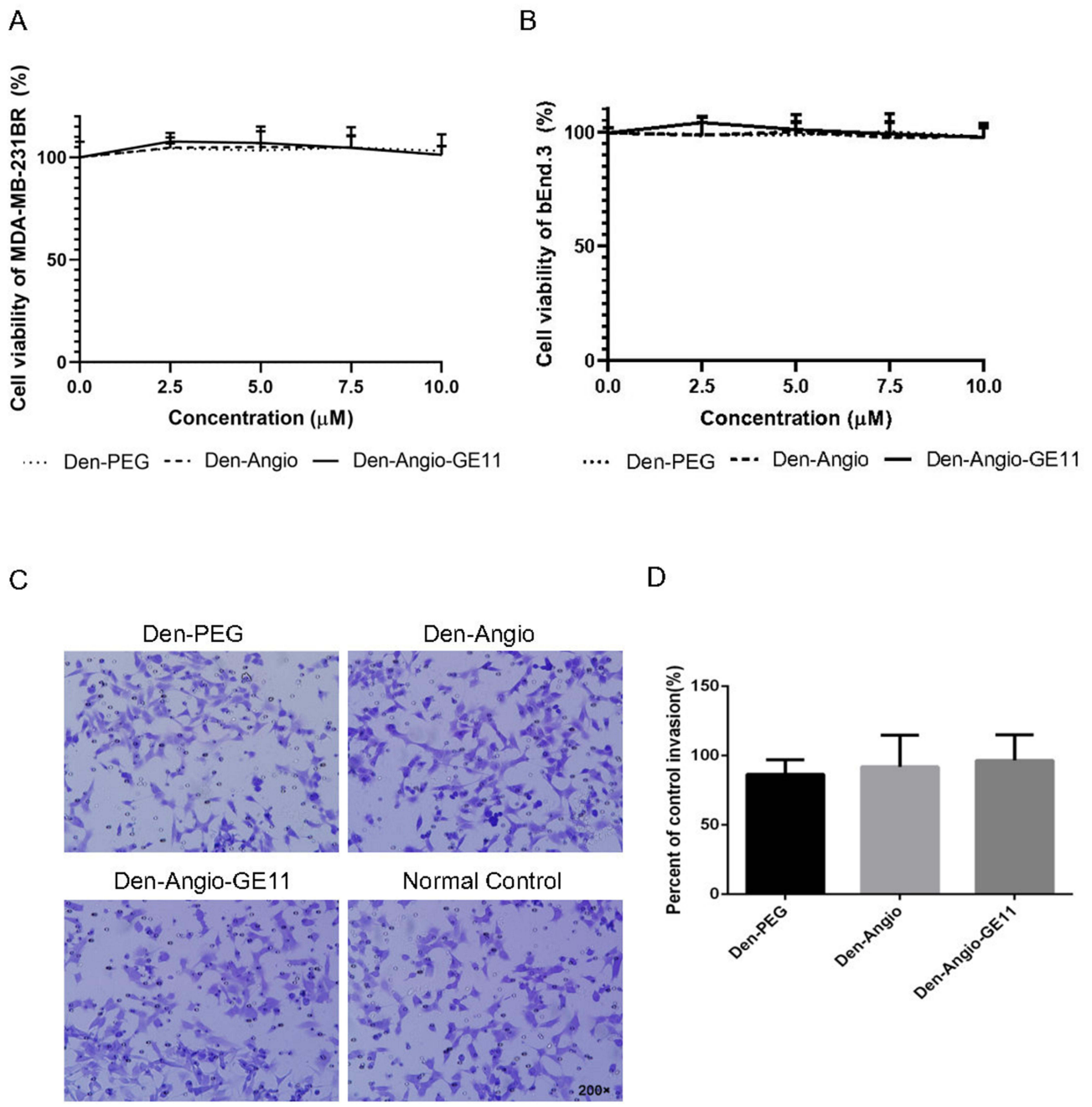

Figure 2 Effects of nanoprobes on the proliferation and invasive ability of cells. (**A**) and (**B**) Effects of Den-Angio-GE11 and its control probe, Den-Angio and Den-PEG on proliferation of Bend.3 (endothelial cells isolated from brain tissue derived from mice) and MDA-MB-231-BR cells. The proliferation viability of bEnd.3 and MDA-MB-231-BR cells was assessed using CCK-8 assay after exposure to various doses of the nanoprobe or its control probes for 48 hours. (n=8) (**C**) Representative images of MDA-MB-231-BR cell invasion in a chamber assay after exposure to Den-Angio-GE11, Den-Angio, or Den-PEG. (**D**) Statistical results of the nanoprobe's effect on cell invasion. (n=4).

Imaging of Early Brain Metastases by Den-Angio-GE11

As Figure 5 shown, early brain metastases could not be enhanced by Gd-DTPA when they were initially detected by T2-weighted MRI. However, significant enhancement was observed following administration of Den-Angio-GE11 on T1-weighted MRI. Similar enhancement was not observed in the control nanoprobe groups (Figure 6A).

In NIRF imaging, the fluorescence signals in the heads were significantly more intense in the Den-Angio-GE11 group than that in the control groups. The signal peaked 2 hours post-administration of the nanoprobes or control vectors and

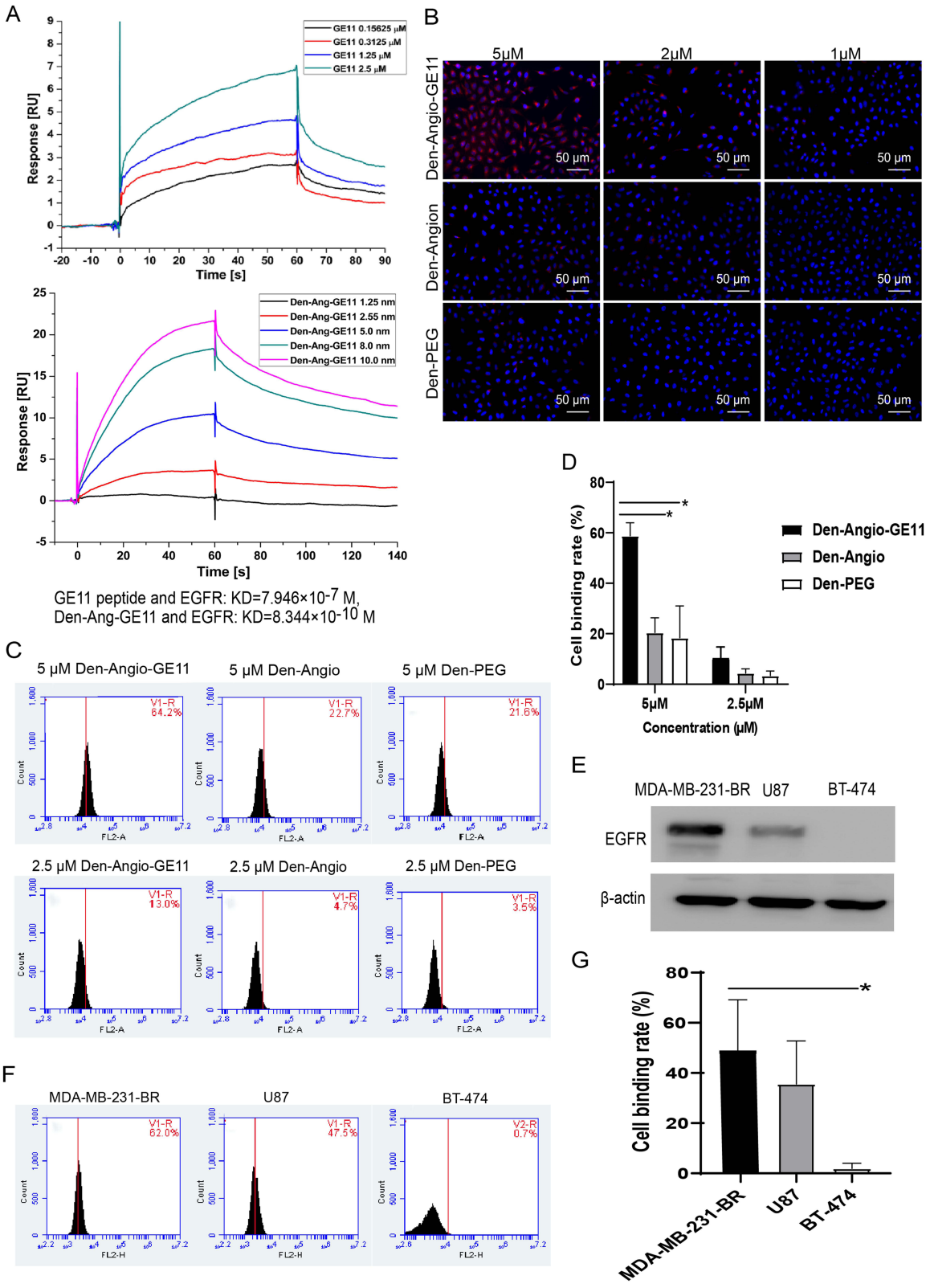

Figure 3 Binding affinity of nanoprobes to EGFR. (**A**) The affinity of Den-Angio-GE11 and GE11 peptide with EGFR protein was directly assayed in vitro by Surface Plasmon Resonance (SPR). The K_D value represents the dissociation constant (M means mol/L). (**B**) Immunofluorescence images of MDA-MB-231-BR cells after incubation with Den-Angio-GE11, Den-Angio and Den-PEG at different concentrations. (**C**) The binding of Den-Angio-GE11 or Den-Angio with MDA-MB-231-BR cells was quantitated by flow cytometry assay. (**D**) Statistics of the binding rate of Den-Angio-GE11 and control nanoprobes. * indicates $p<0.05$, n=3. (**E**) EGFR expression in MDA-MB-231-BR, U87 and BT-474 cells was assayed by Western blotting. (**F**) The binding of Den-Angio-GE11 with MDA-MB-231-BR, U87 and BT-474 cells was assayed by flow cytometry. (**G**) Statistical analysis of the binding rate of Den-Angio-GE11 with MDA-MB-231-BR, U87 and BT-474 cells. * indicates $p<0.05$, n=6.

https://doi.org/10.2147/IJN.S498629

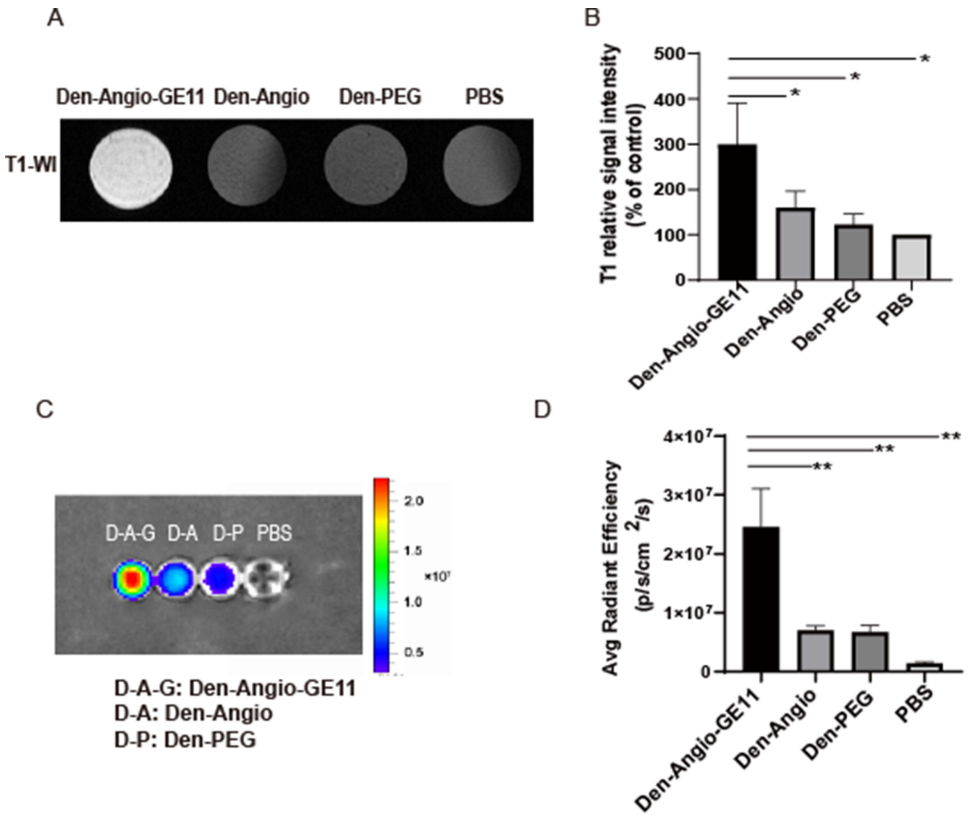

Figure 4 Imaging of nanoprobes targeting MDA-MB-231-BR cells. (**A**) T1-weighted MR imaging of MDA-MB-231-BR cells after incubation with (100 μL and 5 μM) Den-Angio-GE11, Den-Angio, Den-PEG and PBS (5 μM and 100 μL in volume). (**B**) Statistics analysis of T1 signals in MDA-MB-231-BR cells after incubation with Den-Angio-GE11, Den-Angio, Den-PEG and PBS. *indicates $p<0.05$, n=6. (**C**) NIR fluorescence imaging of MDA-MB-231-BR cells after incubation with Den-Angio-GE11, Den-Angio and Den-PEG. (**D**) Statistics analysis of fluorescence signals of MDA-MB-231-BR cells after incubation with Den-Angio-GE11, Den-Angio, Den-PEG and PBS. **indicates $p<0.01$, n=6.

gradually decreased thereafter (Figure 6B and C). The nanoprobes were primarily distributed in the liver and kidneys, with smaller amounts found in the spleen (Figure 6D).

The results of hematoxylin and eosin staining of brain sections confirmed the presence of brain metastases. Examination under a fluorescence microscope showed that Den-Angio-GE11 was enriched in the lesions compared to the Den-Angio control group (Figure 6E).

Imaging of Extreme-Early Brain Metastases by Den-Angio-GE11

Additionally, we imaged extreme-early brain metastases that were undetectable by T2-weighted MRI. As shown in Figure 7A, T2-weighted images did not reveal any significant lesions. After administration of Den-Angio-GE11, although no positive signals were observed on T1-weighted images, NIRF imaging showed significantly higher fluorescence intensity in the BMS group compared to the sham group, regardless of Den-Angio-GE11 presence (the average radiation efficiency value is 46.27×10^6 in BMS group with Den-Angio-GE11, 10.28×10^6 in sham group with Den-Angio-GE11 and 1.31×10^6 without nanoprobe, respectively. $P = 0.005$) (Figure 7B and C).

Histological examination indicated that metastatic cells were dispersed in the brain parenchyma at this stage, with no clusters in the lesions. Most nanoprobes bound to metastatic cells in the BMS group, demonstrated by the overlap of red fluorescence from Den-Angio-GE11 with green fluorescence in metastatic cells. This result demonstrates that Den-Angio-GE11 can cross the BBB and target brain metastatic MDA-MB-231 BR cells in vivo (Figure 7D).

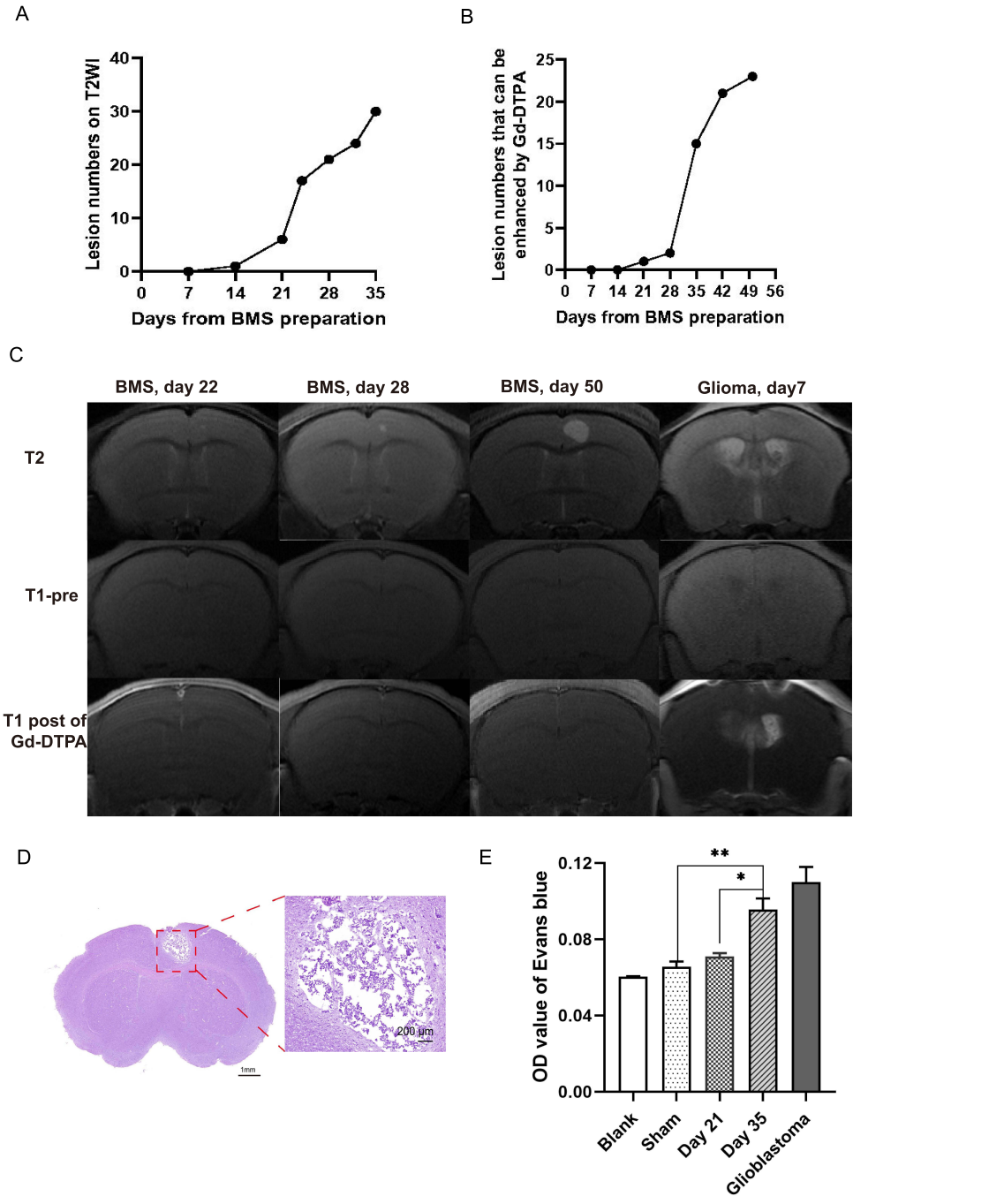

Figure 5 The evolution of BBB permeability during the progression of TNBC brain metastasis. (**A**) The progression of brain metastases was traced by T2-weighted imaging every week. (**B**) The evolution of BBB permeability during the progression of brain metastases was monitored by Gd-DTPA leakage in T1-weighted imaging. (**C**) A representative case with an intact BBB even 50 days after brain metastasis induction. The orthotopic glioma in mice induced by GL261 cells was used as a negative case. (**D**) Histological examination of brain lesions in sections stained with hematoxylin and eosin. (**E**) BBB permeability was also quantified by assessing Evans blue leakage. ** means $p<0.01$ and * means $p<0.05$, n=4.

Discussion

Brain metastasis is devastating, and early detection is crucial for improving patient prognosis. In this study, we developed a nanoprobe, Den-Angio-GE11, capable of crossing the BBB and targeting metastatic cells by conjugating Angiopep-2 and GE11 peptides. The early detection capability of this nanoprobe was evaluated in mouse model of brain metastasis induced by MDA-MB-231-BR cells. Our data indicated that Den-Angio-GE11 significantly enhanced the signals of brain

https://doi.org/10.2147/IJN.S498629

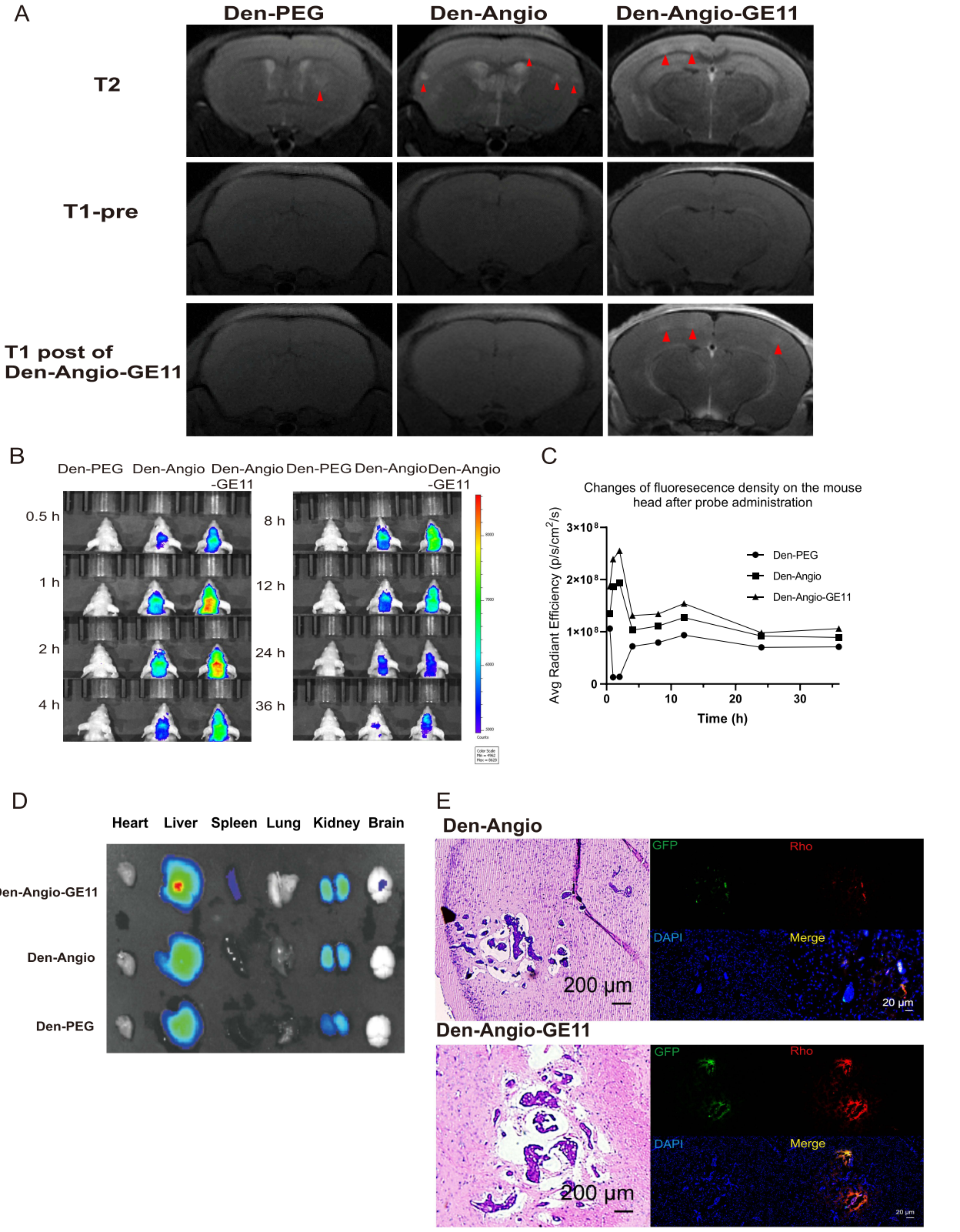

Figure 6 Imaging brain metastases using Den-Angio-GE11 when lesions were detected by T2-weighted MRI. (**A**) Brain metastases were identified in the T2-weighted MRI. In the subsequent week, brain metastases were imaged using T1 sequence of MRI before and after the administration of nanoprobes. "T1-pre" and "T1-post" denote the time points before and after the administration of Den-Angio-GE11 or its control nanoparticles (1 μmol/mouse). T1-enhancement was conducted 1–2 hours after nanoparticles administration. Red arrows mean visible brain metastasis lesions. (**B**) Dynamic investigation of NIR fluorescence imaging on mouse heads after nanoprobes administration. (**C**) Quantification of fluorescence density on mouse heads at different time point after nanoprobe administration. (**D**) Distribution of nanoprobes in organs 36 hours post-administration. (**E**) Histological examination of brain sections. The left images are stained with hematoxylin and eosin, while the right images are immunofluorescence images. Green indicates GFP on metastatic MDA-MB-231-BR cells; red represents rhodamine on Den-Angio-GE11 or control nanoprobes, and Blue depicts DAPI staining for nucleus.

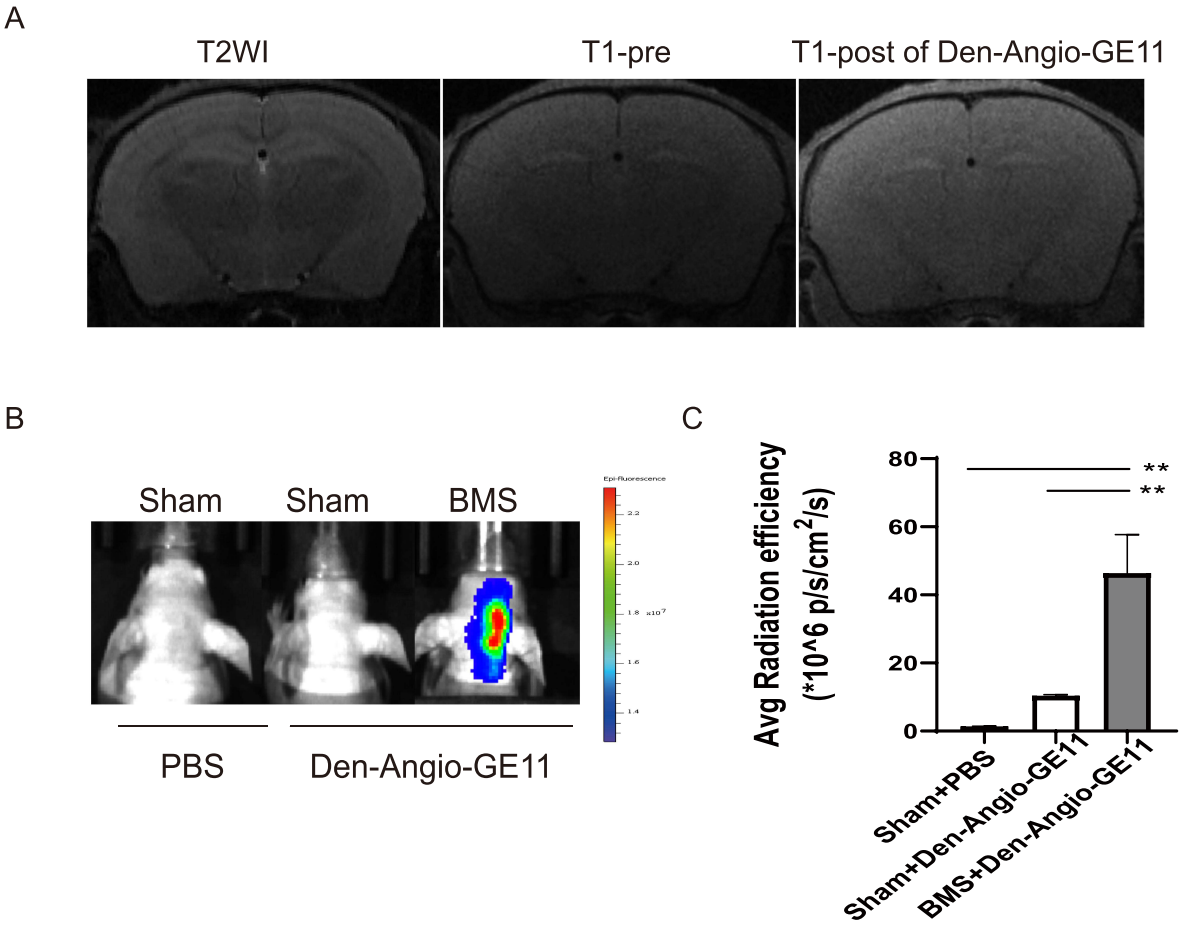

Figure 7 Imaging brain metastases using Den-Angio-GE11 before lesions could be detected by T2-weighted MRI. (**A**) Early brain metastases were imaged by T2 sequence of MRI. T1-enhancement were then conducted using T1 sequence of MRI 2 hours after Den-Angio-GE11 administration (1 μmol/mouse). "T1-pre" and "T1-post" indicate before and after Den-Angio-GE11 administration. (**B**) NIR fluorescence imaging on mouse head 1–2 hours after Den-Angio-GE11 administration (1 μmol/mouse). Mice that underwent sham operation served as a control group. (**C**) Quantification of fluorescence density on mouse heads after Den-Angio-GE11 administration. ** indicates $p<0.01$, n=6–7. (**D**) Immunofluorescence images of brain sections. Green indicates metastatic MDA-MB-231-BR cells; red represents nanoprobe Den-Angio-GE11, and blue depicts nucleus. The Box indicates areas for fluorescence imaging.

https://doi.org/10.2147/IJN.S498629

metastases in the early stage through T1-weighted MRI and NIRF imaging, while Gd-DTPA could not. In the extreme-early stage, when brain metastases were not apparent on T2-weighted MRI, Den-Angio-GE11 enhanced signals of brain metastases on NIRF imaging but not on T1-weighted MRI. Taken together, early TNBC brain metastasis can be detected using Den-Angio-GE11.

The "early stage" in brain metastases lacks a clear definition and definitive quantitative criteria. For instance, human micrometastases are generally defined as lesions less than 2 mm in diameter or comprising fewer than 200 cells, whereas mouse micrometastases consist of no more than 10 cells and lack angiogenesis.[25,26] However, there is no similar definition for the early brain metastasis. In clinic, the gold standard for diagnosis of brain tumors is T1 enhancement in MRI which is based on Gd-DTPA leaking from compromised BBB. However, the average survival of TNBC brain metastases after diagnosis is very short (only 4.9 months),[4,5] implying that they are probably in advanced stage when diagnosed by conventional T1 enhancement in MRI. Therefore, detection of early brain metastases was supposed to occur before BBB compromise in patients.

It is reported brain metastasis induced by MDA-MB-231-BR cells develops slowly.[27] This makes it suitable for imaging or drug delivery study of brain tumors because it provides a long time window for BBB investigation. Indeed, the time of BBB functioning in brain metastasis by MDA-MB-231-BR was obviously longer compared to orthotopic gliomas in this study. Almost all brain metastasis lesions required about three weeks to be detected on 7.0T MR by T2-weighted images, then the BBB still could remain functional for an additional one or two weeks. Even in some individuals, the BBB remained functional for 50 days post-brain metastasis preparation. On the contrary, the orthotopic gliomas by GL261 just kept BBB functional for several days from cells planted in our study.

Detecting early brain metastases requires a good signal-to-noise ratio in imaging. Targeting strategies can enhance probe concentration in lesions, subsequently improving the signal-to-noise ratio of images. However, due to the heterogeneity of triple-negative breast cancer brain metastases, well-known molecular targets for imaging are lacking. EGFR is known to be overexpressed in various tumor types, including triple-negative breast cancer.[10,13,14] Our previous study showed that EGFR plays a significant role in brain metastases of MDA-MB-231-BR cells in mice.[28] In this study, EGFR was significantly overexpressed in MDA-MB-231-BR cells, moderately expressed in U87 cells, and not expressed in BT-474 cells. The probe Den-Angio-GE11 is selectively bound to MDA-MB-231-BR and U87 cells but not BT-474 cells. This specific binding demonstrates the targeting capability of Den-Angio-GE11 for metastatic MDA-MB-231-BR cells in vivo.

Optimizing the efficacy of nanoprobes to traverse the BBB is crucial for enhancing the signal-to-noise ratio. Various factors of probes, such as size, charge properties, and shape, affect their ability to cross the BBB. Among these factors, nanoparticle size significantly affects the ability to cross the BBB. Oshra et al reported that smaller nanoprobes (20–70 nm) exhibit superior BBB penetration capabilities, with Ohta et al identifying that the optimal size for brain entry is 15 nm.[29,30] Additionally, the brain extracellular space (ECS) and interstitial fluid (ISF) drainage within the ECS determine whether a probe can reach its target cells after crossing BBB.[31,32] Given that the physiological ECS in brain tissue is approximately 20 nm, smaller nanoprobes diffuse more efficiently, making enhanced enrichment in metastatic sites and increased signal-to-noise ratios of images.[25,26] Den-Angio-GE11 was 8.8 nm in diameter and significantly outperformed Gd-DTPA in detecting brain metastases on T1-weighted MRI. However, the small size of Den-Angio-GE11 also led to rapid clearance by kidneys and reduced circulation time. Peak fluorescence in brain metastases was observed at 1–2 hours post-administration, followed by a gradual decline. This highlights the challenge of optimizing nanoprobe size for effective BBB penetration while maintaining sufficient circulation time to maximize diagnostic potential.

In clinical settings, MR plain scans are commonly used for screening brain metastases following primary tumor resection or treatment with radiotherapy and chemotherapy. The fact that these extreme-early brain metastases were undetectable by T2-weighted imaging in 7.0T MR suggests that the conventional plain MR scans will also miss those tiny metastases. Therefore, utilizing other highly sensitive imaging techniques is promising for the detection of these extreme-early foci. For example, PET-MR leveraged both high sensitivity and high spatial resolution, so it is probably useful for the detection of extreme-early brain metastases in future.[33]

Although near-infrared fluorescence (NIRF) imaging by Den-Angio-GE11 indicated metastatic lesions and histological examination of brain metastasis specimens confirmed this result, however, the T1-enhancement performance of Den-Angio-GE11 on extreme-early lesions was not ideal. This limitation results from the low cell density in extreme-early foci. Therefore, in addition to the more sensitive imaging modality as mentioned above, more effective techniques to help imaging agents cross

uncompromised BBB are also necessary. In addition, save and effective nanoparticles are promising for clinical transformation. Liposome nanoparticles have been widely used for drug delivery and have been transformed in clinical practice. Recently, Chen et al fused platelet cell membranes with liposomes and targeted tumors that highly expressed CD44 by P-selectin on the surface of platelet membrane. This is an inspiration for us to enhance abilities of crossing BBB and targeting TNBC brain metastasis in future studies.[34]

In this study, the BBB in brain metastasis induced by MDA-MB-231-BR cells in mice exhibited prolonged functions. Den-Angio-GE11, a two-order nanoprobe created by conjugating Angiopep-2 and GE11 peptides to G5 PAMAM dendrimers, successfully crossed the BBB and targeted metastatic MDA-MB-231BR cells in the brain, enhancing the T1 and NIRF signals of brain metastases that just detectable by T2-weighted imaging. However, for extreme-early brain metastases undetectable by T2-weighted imaging, its T1-enhancement effect was limited, highlighting the need for a more sensitive imaging technique or further improve the gadolinium load in the probes to detect extreme-early TNBC brain metastases.

Acknowledgments

We thank Prof. Li Cong and Dr. Gao X.H. of the School of Pharmacy, Shanghai Institute of Infectious Disease and Biosecurity, Fudan University for nanoprobe synthesization.

Author Contributions

All authors made a significant contribution to the work reported, whether that is in the conception, study design, execution, acquisition of data, analysis and interpretation, or in all these areas; took part in drafting, revising or critically reviewing the article; gave final approval of the version to be published; have agreed on the journal to which the article has been submitted; and agree to be accountable for all aspects of the work.

Funding

This work was supported by the National Natural Science Foundation of China (NSFC, Nos. 81301271, 81301870) and Jiangsu Provincial Medical Innovation Center (CXZX202219).

Disclosure

The authors declare no competing interests.

References

1. Lin NU, Claus E, Sohl J, Razzak AR, Arnaout A, Winer EP. Sites of distant recurrence and clinical outcomes in patients with metastatic triple-negative breast cancer: high incidence of central nervous system metastases. *Cancer*. 2008;113(10):2638–2645. doi:10.1002/cncr.23930
2. Malin D, Strekalova E, Petrovic V, et al. αB-crystallin: a novel regulator of breast cancer metastasis to the brain. *Clin Cancer Res*. 2014;20(1):56–67. doi:10.1158/1078-0432.Ccr-13-1255
3. Brosnan EM, Anders CK. Understanding patterns of brain metastasis in breast cancer and designing rational therapeutic strategies. *Ann Transl Med*. 2018;6(9):163. doi:10.21037/atm.2018.04.35
4. Santos J, Arantes J, Carneiro E, et al. Brain metastases from breast cancer. *Clin Neurol Neurosurg*. 2020;197:106150. doi:10.1016/j.clineuro.2020.106150
5. Sperduto PW, Kased N, Roberge D, et al. The effect of tumor subtype on the time from primary diagnosis to development of brain metastases and survival in patients with breast cancer. *J Neurooncol*. 2013;112(3):467–472. doi:10.1007/s11060-013-1083-9
6. Guo Q, Zhu Q, Miao T, et al. LRP1-upregulated nanoparticles for efficiently conquering the blood-brain barrier and targetedly suppressing multifocal and infiltrative brain metastases. *J Control Release*. 2019;303:117–129. doi:10.1016/j.jconrel.2019.04.031
7. Habib S, Singh M. Angiopep-2-Modified Nanoparticles for Brain-Directed Delivery of Therapeutics: a Review. *Polymers*. 2022;14(4):712. doi:10.3390/polym14040712
8. Bertrand Y, Currie JC, Poirier J, et al. Influence of glioma tumour microenvironment on the transport of ANG1005 via low-density lipoprotein receptor-related protein 1. *Br J Cancer*. 2011;105(11):1697–1707. doi:10.1038/bjc.2011.427
9. Sabbah DA, Hajjo R, Sweidan K. Review on Epidermal Growth Factor Receptor (EGFR) Structure, Signaling Pathways, Interactions, and Recent Updates of EGFR Inhibitors. *Curr Top Med Chem*. 2020;20(10):815–834. doi:10.2174/1568026620666200303123102
10. Sukumar J, Gast K, Quiroga D, Lustberg M, Williams N. Triple-negative breast cancer: promising prognostic biomarkers currently in development. *Expert Rev Anticancer Ther*. 2021;21(2):135–148. doi:10.1080/14737140.2021.1840984
11. Park HS, Jang MH, Kim EJ, et al. High EGFR gene copy number predicts poor outcome in triple-negative breast cancer. *Mod Pathol*. 2014;27(9):1212–1222. doi:10.1038/modpathol.2013.251
12. Hohensee I, Lamszus K, Riethdorf S, et al. Frequent genetic alterations in EGFR- and HER2-driven pathways in breast cancer brain metastases. *Am J Pathol*. 2013;183(1):83–95. doi:10.1016/j.ajpath.2013.03.023

13. Masuda H, Zhang D, Bartholomeusz C, Doihara H, Hortobagyi GN, Ueno NT. Role of epidermal growth factor receptor in breast cancer. *Breast Cancer Res Treat*. 2012;136(2):331–3345. doi:10.1007/s10549-012-2289-9
14. Takeda M, Nakagawa K. Role of EGFR Monoclonal Antibodies in the Management of Non-small Cell Lung Cancer. *Curr Cancer Drug Targets*. 2015;15(9):792–802. doi:10.2174/1568009615091511101430O1
15. Ashton JR, Gottlin EB, Patz EF Jr, West JL, Badea CT. A comparative analysis of EGFR-targeting antibodies for gold nanoparticle CT imaging of lung cancer. *PLoS One*. 2018;13(11):e0206950. doi:10.1371/journal.pone.0206950
16. Gao M, Su H, Lin G, et al. Targeted imaging of EGFR overexpressed cancer cells by brightly fluorescent nanoparticles conjugated with cetuximab. *Nanoscale*. 2016;8(32):15027–15032. doi:10.1039/c6nr04439e
17. Li Z, Zhao R, Wu X, et al. Identification and characterization of a novel peptide ligand of epidermal growth factor receptor for targeted delivery of therapeutics. *FASEB J*. 2005;19(14):1978–1985. doi:10.1096/fj.05-4058com
18. Song S, Liu D, Peng J, et al. Peptide ligand-mediated liposome distribution and targeting to EGFR expressing tumor in vivo. *Int J Pharm*. 2008;363 (1–2):155–161. doi:10.1016/j.ijpharm.2008.07.012
19. Chariou PL, Lee KL, Wen AM, Gulati NM, Stewart PL, Steinmetz NF. Detection and imaging of aggressive cancer cells using an epidermal growth factor receptor (EGFR)-targeted filamentous plant virus-based nanoparticle. *Bioconjug Chem*. 2015;26(2):262–269. doi:10.1021/bc500545z
20. Yamada H, Hasegawa Y, Imai H, et al. Magnetic resonance imaging of tumor with a self-traceable phosphorylcholine polymer. *J Am Chem Soc*. 2015;137(2):799–806. doi:10.1021/ja510479v
21. Matsumura Y, Maeda H. A new concept for macromolecular therapeutics in cancer chemotherapy: mechanism of tumoritropic accumulation of proteins and the antitumor agent smancs. *Cancer Res*. 1986;46(12):6387–6392.
22. Maeda H. The enhanced permeability and retention (EPR) effect in tumor vasculature: the key role of tumor-selective macromolecular drug targeting. *Adv Enzyme Regul*. 2001;41(1):189–207. doi:10.1016/s0065-2571(00)00013-3
23. Sharma AK, Gothwal A, Kesharwani P, Alsaab H, Iyer AK, Gupta U. Dendrimer nanoarchitectures for cancer diagnosis and anticancer drug delivery. *Drug Discov Today*. 2017;22(2):314–326. doi:10.1016/j.drudis.2016.09.013
24. Yan H, Wang L, Wang J, et al. Two-order targeted brain tumor imaging by using an optical/paramagnetic nanoprobe across the blood brain barrier. *ACS Nano*. 2012;6(1):410–420. doi:10.1021/nn203749v
25. Chrabaszcz K, Jasztal A, Smęda M, et al. Label-free FTIR spectroscopy detects and visualizes the early stage of pulmonary micrometastasis seeded from breast carcinoma. *Biochim Biophys Acta Mol Basis Dis*. 2018;1864(11):3574–3584. doi:10.1016/j.bbadis.2018.08.022
26. Rosen PP, Saigo PE, Braun DW, Weathers E, Fracchia AA, Kinne DW. Axillary micro- and macrometastases in breast cancer: prognostic significance of tumor size. *Ann Surg*. 1981;194(5):585–591. doi:10.1097/00000658-198111000-00006
27. Huang Z, Yu P, Tang J. Characterization of Triple-Negative Breast Cancer MDA-MB-231 Cell Spheroid Model. *Onco Targets Ther*. 2020;13:5395–5405. doi:10.2147/ott.S249756
28. Nie F, Yang J, Wen S, et al. Involvement of epidermal growth factor receptor overexpression in the promotion of breast cancer brain metastasis. *Cancer*. 2012;118(21):5198–5209. doi:10.1002/cncr.27553
29. Betzer O, Shilo M, Opochinsky R, et al. The effect of nanoparticle size on the ability to cross the blood-brain barrier: an in vivo study. *Nanomedicine*. 2017;12(13):1533–1546. doi:10.2217/nnm-2017-0022
30. Ohta S, Kikuchi E, Ishijima A, Azuma T, Sakuma I, Ito T. Investigating the optimum size of nanoparticles for their delivery into the brain assisted by focused ultrasound-induced blood-brain barrier opening. *Sci Rep*. 2020;10(1):18220. doi:10.1038/s41598-020-75253-9
31. Ziqi Gu HC, Zhao H, Yang W, et al. New insight into brain disease therapy: nanomedicines-crossing blood–brain barrier and extracellular space for drug delivery. *Expert Opin Drug Deliv*. 2022;19(12):1618–1635. doi:10.1080/17425247.2022.2139369
32. Naseri Kouzehgarani PK G, Bolin SE, Reilly EB, Lefebvre DR, Lefebvre DR. Biodistribution Analysis of an Anti-EGFR Antibody in the Rat Brain: validation of CSF Microcirculation as a Viable Pathway to Circumvent the Blood-Brain Barrier for Drug Delivery. *Pharmaceutics*. 2022;14 (7):1441. doi:10.3390/pharmaceutics14071441
33. Borja AJ, Saini J, Raynor WY, et al. Role of Molecular Imaging with PET/MR Imaging in the Diagnosis and Management of Brain Tumors. *PET Clin*. 2022;17(3):431–451. doi:10.1016/j.cpet.2022.03.002
34. Chen H, Luo X, Huang Q, et al. Platelet membrane fusion liposome loaded with type I AIE photosensitizer to induce chemoresistance cancer pyroptosis and immunogenic cell death for enhancing cancer immunotherapy. *Chem Eng J*. 2023;476:146276. doi:10.1016/j.cej.2023.146276